Technische Universität München

Technische Universität München
Fakultät für Elektrotechnik und Informationstechnik
Professur für Computational Photonics
Prof.Dr.-Ing. Christian Jirauschek

Coupled Transmission Line/Maxwell-Bloch Equations Approach for Electro-Optical Simulations of Terahertz Quantum Cascade Lasers

MASTER THESIS

by Longwei Zhong

April, 2017

Abstract

Quantum cascade lasers (QCLs) are compact, electrically pumped semiconductor devices, which are considered to be promising light source for mid-infrared and terahertz radiation. Benefit from this special mechanism they can utilize the electric power more efficiently than other diode lasers and achieve a high output power. Despite its practical significance, generating ultra short pulses from QCLs by mode-locking has achieved only limited success in the past decade. In this work, we study the influence of external source on the mode-locking of QCLs. A dynamic model based on Maxwell-Bloch equations as well as transmission line was build to simulate QCLs in time domain. The simulation results were then analyzed and compared with existing experiment results from references to check reliability of the established model.

The purpose of this research is to build a new model based on existed simulation methods to achieve a dynamic modeling of QCLs in time domain, which would help to get a better understanding of its theoretical mechanism and redound to search for optimal parameters of mode-locking in experiments.

Acknowledgements

Thanks to Petar

I dedicate this work to my beloved mother and father

List of Symbols

Contents

1 Introduction

The operating principle of QCLs was first proposed by R.F. Kazarinov and R.A. Suris in 1971 [1]. However, due to the complexity of fabrication process until 1994 QCLs was firstly demonstrated at Bell Laboratories by Jerome Faist and his colleagues [2]. They have gained considerable attention afterwards. Unlike common semiconductor lasers, which utilize electron-hole recombination to realize electromagnetic radiation, QCLs are unipolar and their emission is based on intersub- band transitions in coupled quantum well superlattices [3]. Due to lack of suitable radiation sources and detectors this region remains one of the least developed spectral regions. The occurance of QCLs provides a option as a prominent source to help investigate these regions, because their emission wave length as well gain spectrum can be engineered through various design [4]. To date, only n-type QCLs are successfully realized lasing. One of the most commonly used material combination for active region is GaAs (well) and $Al_xGa_{1-x}As$ (barrier), where x is the relative amount ration of aluminum to gallium. The intersubband transmission occurs in conduction band, as Fig. shows. Add–> one module of repeated QCL heterostructures!

As a novel type of laser as well as efficient source to generate THz radiation, THz QCLs showed great potential and have attracted already a lot attentions for developing their possible applications. Compared to X-ray, THz radiation has lower energy ($E = h\nu$), but still can penetrate many materials (e.g. clothes, paper) except for metals. Therefore, it could be used as imaging and sensing for security detection in airport [5], which wouldn't affect the health of our bodies. Another interesting area is astronomy, such as heterodyne receivers [3], which requires THz QCLs. Because the radiation from universe is mainly with THz, the research of THz technologies would help to detect and observe those unnoticed radiation from galaxies.

1.1 Background and motivation

For the past decade since the fist demonstration of QCLs, some groups devoted themselves to improve the operation temperature, up to room temperature has been achieved [6] through special wells design of QCL structure. Some consisted on generating short pulse with QCLs [7]. Active mode-locking was recognized as the only viable route to

QCL mode-locking [8]. The main idea is to lock modes through a modulated injection current with a frequency corresponding to the roundtrip frequency. THz QCLs can be injection locked by modulating a short section of the cavity to open a net gain window with an external RF source. They are biased close to their threshold, while high above threshold pulses are broadened due to multi-mode instabilities (Spatial Hole Burning and Risken-Nummedal-Graham-Haken instability [9]). It was found that mode-locking in THz QCLs is easier than that in mid-infrared [7]. Compared with mid-infrared QCLs, the laser transition energy lies below the optical phonon energy, so the upper state of THz QCLs based on bound-to-continuum has generally longer non-radiative relaxation time ($\sim$ 5-10 ps), which makes it easier to realize mode-locking [10]. The first successful attempt of mode-locking in THz QCLs was reported in 2010 [11]. By direct amplitude modulation, the mode-locking of a 2.3THz QCL was achieved at 35GHz, which shows locking ranges up to $\sim$225MHz [11]. Recently, active mode locking of QCLs in an external ring cavity was reported [8], which can operate at room temperature. Moreover, benefits from this method, the mode-locking was observed not only at close to the threshold, but also far above it.

Although there are already those successful experimental attempts by active mode-locking, but a complete theory system is still not available. Due to limited knowledge of unfavorable physical effects and lack of consolidation theory about its mechanism, it has been proven to be difficult to directly employ existing techniques from the ultra fast optics community to realize mode-locking of QCLs.

1.2 Related work

Accompanied with experimental research, modeling techniques for QCLs are also steady investigated to help get a deep understanding of internal mechanisms and explore unknown effects. Thanks for persistent efforts of researchers, there are already several models as well as solvers which could be used for describing and analyzing various of processes in QCLs, such as density matrix approach, Maxwell-Bloch equations, non-equilibrium Green's function theory along with some other modified methods aimed to take more linearities and effects into account. These models have been used, for example, to investigate modulation properties of optical injection-locked QCLs [12], to calculaton for four-level scheme THz QCLs [13].

However, these exsisting simulation techniques are only able to find solution of steady states rather than dynamic modeling in time domain. A lumped-element approach was proposed in 2007 by Barbieri et al. to investigate amplitude modulation limit [14]. After that this concept has been further developed with distributed-parameter transmission-line simulations to quantify injected RF-power to QCLs [15]. With the aid of a vectorial network analyzer they measured the S-parameters of meta-metal

waveguides THz QCLs which were driven under threshold and then extracted distributed parameter from S-parameters. This is the first attempt that by measuring the transmission and reflection coefficients and using transmission-line approach to analyze RF-modulation capabilities of THz QCLs.

1.3 Objective

The objectives of this thesis are as follows:

1). To build a new dynamic model based on Transmission line

2). To verify "pulling effect" in mode-locking through simulation

3). To acquire optimal simulation parameters to generate short pulse

4). To gain a deep understanding of mode-locking behaviors to obtain a better design in the future.

2 Theory

QCL is composed of a great amount of repeated stacks of heterojunctions, its extreme thin layers (in the order of a few nanometers) of different materials result in the formation of quantum wells and barriers. By solving steady Schroedinger-Poisson equation system, eigenenergies and wave functions of eigenenergies can be determined, which help to engineer and optimize QCLs (e.g. radiation frequency, injection efficiency). Transfer matrix method [16] and finite-difference method [17] are widely used to compute the numerical solution of the system efficiently.

2.1 Maxwell-Bloch equations

To describe carrier dynamics as well as light propagation in a laser, Maxwell-Bloch equations can be used as a empirical approach. ****–>Introduction of FL183S Maxwell's equations–>explaination of the equation

Bloch equations–>3 levels for example

2.2 Transmission line

Transmission line model was created by Oliver Heaviside [18] and usually consists of two separated conductors and medium in between (Fig. 2.1). The conventional TLM is based on Telegrapher's equations (2.1)(2.2), which describe the evolution of voltage and current both spacial and temporal on an electrical transmission line. These two differential equations contains four distributed components (R', L', G', C') which vary from different transmission lines: R' is distributed resistance of conductors, which is represented by a series resistor in ohms per unit length (Ω/m); L' is distributed inductance resulting from the magnetic field around the line due to self-inductance, which is represented by a series inductor in henries per unit length (H/m); G' is distributed conductance of the dielectric material separating the two conductors, which is expressed in siemens per unit length (S/m) and represented by a shunt resistor with resistance of $1/G'$; C' is distributed capacitance of transmission line, which is represented by a shunt conductor in farads per unit length (F/m).

Transmission line can be further classified in lossy/non-lossy transmission line and uniform/nonuniform transmission line with regarding to characteristics of its conductors and medium. When no resistance (idea conductor) and conductance (idea dielectric medium) exist, it can be regarded as ideal transmission line which contains only L' and G'. In uniform transmission line all those distributed components are uniformly distributed along line. Therefore, under the assumptions above the simulated QCL can be defined as a 1D nonlinear lossy transmission line.

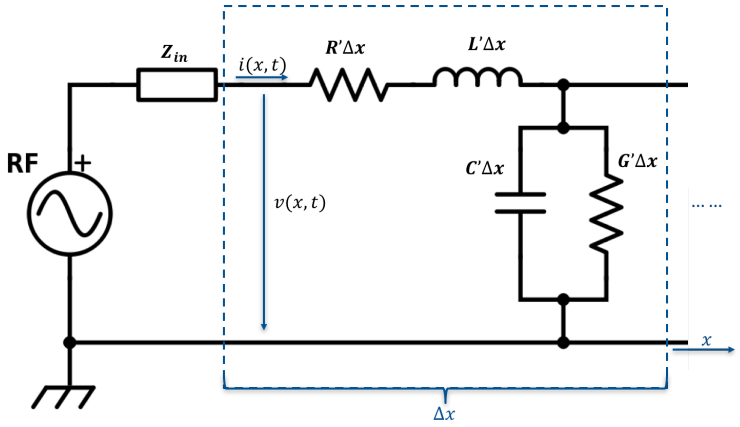

Figure 2.1: *: An equivalent circuit representation of a differential section of the waveguide with capacitance per unit length C′ and inductance per unit length L′.*

Telegrapher's equations:

$$\frac{\partial v(x,t)}{\partial x} = -L'\frac{\partial i(x,t)}{\partial t} - R'i(x,t) \tag{2.1}$$

$$\frac{\partial i(x,t)}{\partial x} = -C'\frac{\partial v(x,t)}{\partial t} - G'v(x,t) \tag{2.2}$$

2.3 Mode-locking

Light generated by lasers owns high coherent compared with from other light sources. Nevertheless, it has still large bandwidth of optical gain, the modes inside cavity osculate independently and don't have fix phase, which leads to wide pulse. By uncertainty principle, if pulse duration is quite short, its bandwidth muss be larger. For example, a hyperbolic-secant-squared pulse shape is often assumed for lasers generating ultrashort pulse, the minimum possible pulse duration Δt can be calculated with

$$\Delta t = \frac{0.315}{N\Delta\nu}. \tag{2.3}$$

Where 0.315 is pulse shape dependent time bandwidth product, which for Gaussian shape pulse is 0.441. N and $\Delta\nu$ is amount of modes and bandwidth of pulse, respec-

tively. This formula above could be be used for roughly evaluating the shortest possible pulse width. However, in real case, many other factors have to be taken into consideration, such as dispersion of the cavity, pulse shape and so on.

Mode-locking is a technique in optics, which locks multi-mode in resonant laser cavity by enforcing coherence between modes to produce extra short pulse[19]. Methods of mode-locking can be simply classified as active mode-locking (AML) and passive mode-locking(PML) depending on whether it is induced by itself (e.g. absorber) or requires external source (e.g. RF source).

fundamentals of mode-locking knowledge: FP, locking range, modes..... Ideally it is exactly at f_{tr}, but even if modulated at frequency of a little variation with f_{tr}, the laser could still be mode-locked, the maximal possible frequency interval is called locking range.

3 Model

The dynamic model consists of two parts. One of them is optical modeling, which is used for describing the carrier transport as well as light propagation inside cavity (microcosmic). The other is based on transmission line to obtain voltage and current distribution along cavity (microcosmic). Although each of them has separate solver, both will be simulated simultaneously and can affect with each other.

3.1 Optical modeling

Similar with the existing modeling methods, in this model light propagation is described with Maxwell' equation while carrier transportation is determined by Bloch equation. Without regard to lateral non-uniform distribution at boundaries [20, 21] QCL can be simplified to one-dimensional (1D) structure in the direction of propagation (x axis), which means the electrical components were uniformly distributed throughout the cross-sectional area.

3.1.1 Carrier transport

To simulate QCL active regions, we adapt the density matrix model from Ref. [cite Belyanin], to include total of four subband levels, and more importantly to allow all relevant system parameters, such as the eigenenergies, dipole moments and all scattering rates to be bias dependent.

As a prototypical QCL design, we take the sub-band structure configuration illustrated in Fig. 3.1, consisting of 4 relevant levels per period, i.e. levels from 1 to 4, where level 4 denotes the upper laser state, level 3 the lower laser level, level 2 is an extraction level which eases the electron extraction from 3, and finally level 1 denotes the depopulation level of the period, which also coincides with the injector state (1') of the next module. Typical QCL designs consist of more than 30 repetitions of this schematic, however we can employ periodic boundary conditions [cite] and restrict our attention to a single period only.

The time evolution of the density matrix is given by the von Neumann equation, which we couple to a wave equation for $E_z(x,t)$, denoting the z-component electric

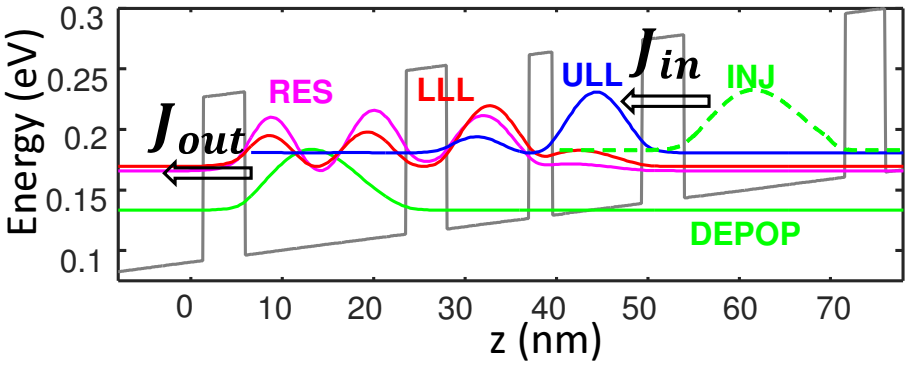

Figure 3.1: *Sub-band structure configuration of QCL.*

field (and also the assumed laser growth direction).

$$\frac{d\rho_{44}}{dt} = J + i\frac{ez_{43}}{\hbar}E_z(\rho_{43} - \rho_{34}) + \sum_{j\neq 4}\frac{\rho_{jj}}{\tau_{j\to 4}} - \frac{\rho_{44}}{\tau_4}, \tag{3.1a}$$

$$\frac{d\rho_{33}}{dt} = -i\frac{ez_{43}}{\hbar}E_z(\rho_{43} - \rho_{34}) + \sum_{j\neq 3}\frac{\rho_{jj}}{\tau_{j\to 3}} - \frac{\rho_{33}}{\tau_3}, \tag{3.1b}$$

$$\frac{d\rho_{22}}{dt} = \sum_{j\neq 2}\frac{\rho_{jj}}{\tau_{j\to 2}} - \frac{\rho_{22}}{\tau_2}, \tag{3.1c}$$

$$\frac{d\rho_{11}}{dt} = -J + \sum_{j\neq 1}\frac{\rho_{jj}}{\tau_{j\to 1}} - \frac{\rho_{11}}{\tau_1}, \tag{3.1d}$$

$$\frac{d\rho_{43}}{dt} = -i\omega_{43}\rho_{43} + i\frac{ez_{43}}{\hbar}E_z(\rho_{44} - \rho_{33}) - \Gamma_{\|43}\rho_{43}. \tag{3.1e}$$

In Eqs. (3.1) ρ_{ij} denotes the $ij-$th density matrix element, z_{43} the optical transition's dipole moment, e the elementary charge, $\hbar$ is the reduced Plank's constant. Also the parameter $1/\tau_{i\to j}$ is the net scattering rate from level i to level j, calculated by our ensemble Monte Carlo code and incorporating, amongst others, longitudinal optical (LO) phonon, interface roughness and electron electron scattering mechanisms [cite]. Lastly $1/\tau_i = \sum_j 1/\tau_{i\to j}$ is the inverse lifetime of level i and $\Gamma_{\|43} = (\tau_4 + \tau_3)/(2\tau_4\tau_3) + 1/\tau^*$ is the dephasing rate of the optical transition, including lifetime broadening and a phenomenological pure dephasing $1/\tau^*$ rate due to intrasubband scattering processes [cite ANDO model]. The only scattering mechanism treated quantum mechanically is the optical transition between the upper and lower laser states. One can also fully coherently include resonant tunneling between the injector 1' and the upper laser state 4, which leads to a modified system of equations with larger number of independent variables and is thus more computationally demanding [cite]. Furthermore such an approach does not allow for the inclusion (without $k-$space discretization) of second order tunneling current into the simulations, which has been shown to be the origin of negative the differential conductivity and dispersive gain in quantum cascade

lasers []. This is why in this publication we adhere to the more intuitive model from [cite Belyanin], which can be easily adapted to include various models for the current density via the term J in the above equations. Keeping in foresight that we would like to couple the density matrix equations to an electrical model for the waveguide, we find the later model as the more suitable alternative.

In the tight-binding basis [cite], we can assume that the only electron transport channel across the QCL periods is via the resonant tunneling current between the injector and the upper laser state. When second order scattering effects are considered, under a few relaxing approximations, this tunneling current is given by [cite Terrazzi]

$$J = en^s \frac{\Omega_{AC}^2 2\Gamma_{\parallel 1'4}}{\epsilon^2 + 4\Gamma_{\parallel 1'4}^2} \Big\{ \Theta(\epsilon)(\rho_{11} - \rho_{44} e^{-|\hbar\epsilon|/k_B T}) + \Theta(-\epsilon)(\rho_{11} e^{-|\hbar\epsilon|/k_B T} - \rho_{44}) \Big\}. \tag{3.2}$$

In Eq. (3.2) n^s denotes the sheet carrier density, $\Theta(\,\cdot\,)$ is the Heaviside function and the term $e^{-|\hbar\epsilon|/k_B T}$ denotes an effective "weight" factor modelling the assumption of thermalized k-space distribution of the injector and upper laser level electrons with the same thermal energy $k_B T$ in each subband.

3.1.2 Light propagation

****–>rewrite, give more explanation for concept polarization P

In order to include the electric field dynamics into the overall picture, we write down the inhomogeneous wave equation

$$\left[\frac{c^2}{n_{THz}^2} \frac{\partial^2}{\partial x^2} - \frac{\partial^2}{\partial t^2} \right] E_z = \frac{1}{\epsilon_0 n_{THz}^2} \frac{\partial^2}{\partial t^2} P, \tag{3.3}$$

where n_{THz} denotes the background refractive index of the bulk active region, c is the velocity of light in vacuum and ϵ_0 is the permittivity of free space. The symbol P denotes the (nonlinear) polarization of the two level system and is given by

$$P(x,t) = -\frac{n^s}{L_p} \Gamma e z_{43} (\rho_{43} + \rho_{34}), \tag{3.4}$$

with Γ is the field confinement factor and L_p is the period length.

For the final set of equations, we also employ the rotating wave and slowly varying envelope approximations [cite], which allows us to reduce the wave equation (3.3) to a pair of propagation equations, an also eliminate fast oscillating terms from the density matrix equations (3.1). The corresponding final formulas are slightly modified versions of those in [cite me, cite belyanin], and therefore we omit them here

for brevity. We would like to point out also that in all subsequent calculations, we have also taken into consideration the effect of the inversion grating on to the current density, in an analogous manner to [cite belyanin].

3.2 Electrical modeling

In the electrical modeling, a modified Transmission Line Method (TLM) was introduced in order to realize a dynamic modeling in time domain. TLM is a very efficient methode which is already widely used for evaluation and dynamic modeling especially in high frequency region where wave nature muss be taken into accout, for example, contact resistance extraction in organic field- effect transistors [22], dynamic modeling of flow in pipelines [23] etc. However, in QCLs are transverse magnetic (TM) modes [24] while TLM is specially for analysis of transverse electromagnetic (TEM) modes, in which neither electric nor magnetic field in the direction of propagation. The common used metal-metal waveguide (microstrip structure) in QCLs can be regarded as quasi-TEM structure, as the substrate ($\sim$ 10 um) is quite thin in terms of wavelength (30 mm $\sim$ 300 mm), and the width of strip conductor is very narrow ($\sim$ 50 um) in terms of wavelength as well, therefore, a static analysis should be still perfectly adequate in this case.

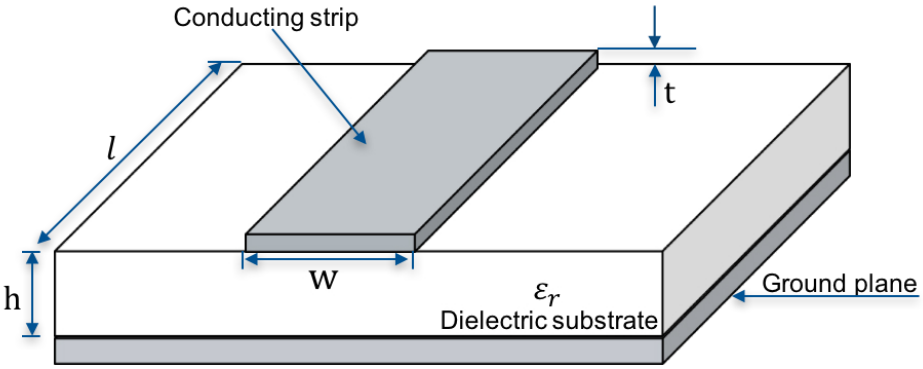

Figure 3.2: *Microstrip structure.*

3.2.1 Transmission line approach

In this model, the vertical current component resulting from conductance of active region (n-doped semiconductor) under bias is calculated by current density J'(x,t) rather than by distributed conductance G'. Current density J(x,t) is nonuniform and bias dependent, it will be obtained by carrier transmission in optical part. Furthermore, although $v(x,t)$ and $i(x,t)$ in Eq. (2.1) and (2.2) are special for high frequency signal,

they will be still valid if the transmission line was supplied additionally with a dc source. Therefore, the Telegrapher equations will be modified as following:

$$\frac{\partial v(x,t)}{\partial x} = -L'\frac{\partial i(x,t)}{\partial t} - R'i(x,t) \tag{3.5}$$

$$\frac{\partial i(x,t)}{\partial x} = -C'\frac{\partial v(x,t)}{\partial t} - wJ'(x,t). \tag{3.6}$$

where, v(x,t) and i(x,t) are voltage and current signal at a node

Boundary conditions

Boundary conditions account for the completeness of differential equations at the boundary. In order to refine the boudaries and avoid hard variation of electrical components, a cascading of π networks[25] is introduced for the distributed transmission line by splitting the shunt capacitance and conductance in half with two parallel capacitors and conductors at boundary, which is illustrate in Fig. 3.3.

In active mode-locking, QCL is supplied with source V_S which consists of a DC voltage source V_{DC} and an external RF source V_{RF}. These two sources are combined through bias-T and the source voltaged can be expressed with $V_S = V_{DC} + V_{RF}$. As the right side of QCL lefts open, no current component exists at the end node. Consequently, the boundary condition for current is definitely $I^n_{end} = 0$. Besides, due to existance of wire impedance (50 Ω) there will be voltage drop on it, so the voltage at node 0 is not equal to source voltage V_S.

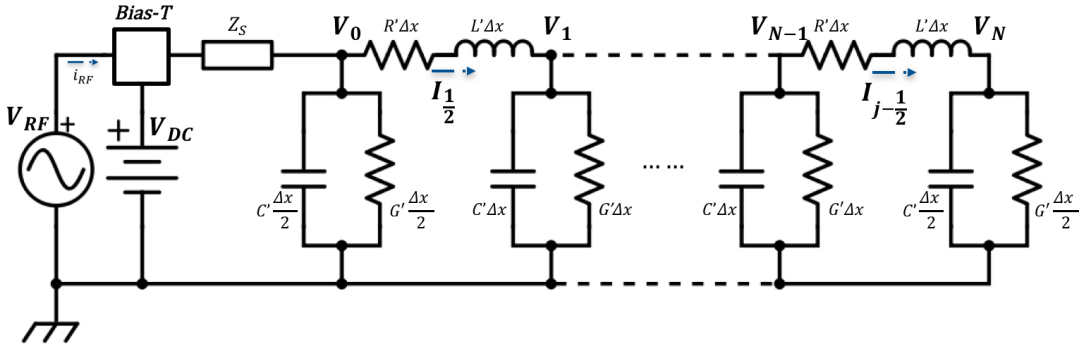

Figure 3.3: *Schematic of cascade π network representation and Thévenin equivalent circuit. Error: $I_{N-\frac{1}{2}}$*

By using Kirchhoff's voltage law (KVL),

$$V^n_{RF} + V_{DC} = Z_S\widetilde{i}^n_{-\frac{1}{2}} + V^n_0 \tag{3.7}$$

where $\widetilde{i}^n_{-\frac{1}{2}}$ denotes ac component among whole current after bias-T and before node 0. The same as in transmission line equation, it can not be directly calculated during iterative process. So by applying the same approximation treatment $\tilde{i}^{n+1}_{-\frac{1}{2}} - \tilde{i}^n_{-\frac{1}{2}} \approx I^{n+1}_{-\frac{1}{2}} - I^n_{-\frac{1}{2}}$, Eqn. (3.7) will be transformed to:

$$V^{n+1}_{RF} - V^n_{RF} = V^{n+1}_0 - V^n_0 + Z_S(I^{n+1}_{-\frac{1}{2}} - I^n_{-\frac{1}{2}}) \tag{3.8}$$

The injected current to QCL can be calculated through Kirchhoff's current law (KCL), at node 0:

$$I^{n+1}_{-\frac{1}{2}} - I^n_{-\frac{1}{2}} = I^{n+1}_{\frac{1}{2}} - I^n_{\frac{1}{2}} + C'\frac{\Delta x}{2}(\frac{\partial V^{n+1}_0}{\partial t} - \frac{\partial V^n_0}{\partial t}) + w\frac{\Delta x}{2}(J^{n+1}_0 - J^n_0) \tag{3.9}$$

Substitute Eqn. 3.9 into Eqn. 3.8, and then rearrange the equation to get an explicit update expression at boundary:

$$\begin{aligned} V^{n+\frac{3}{2}}_0 = \frac{2Z_SC'\Delta x}{Z_SC'\Delta x + \Delta t}V^{n+\frac{1}{2}}_0 + \frac{\Delta t - Z_SC'\Delta x}{Z_SC'\Delta x + \Delta t}V^{n-\frac{1}{2}}_0 + \frac{2\Delta t}{Z_SC'\Delta x + \Delta t}\big[V^{n+1}_{RF} - V^n_{RF}\cdots \\ -Z_S\big(I^{n+1}_{\frac{1}{2}} - I^n_{\frac{1}{2}} + w\tfrac{\Delta x}{4}(J^{n+\frac{3}{2}}_0 - J^{n-\frac{1}{2}}_0)\big)\big] \end{aligned} \tag{3.10}$$

OR:∗∗

Use 40 GHz low loss RF coaxial cable which has 50 Ohms impedance.

$Z_S = \sqrt{\frac{L}{C}} = 50\Omega$ (C = 27 pF/ft, L = 6.75e4 pH/ft, one foot length, 1 foot = 0.3048 m)

By using Kirchhoff's law,

$$V^{n+\frac{1}{2}}_S - V^{n+\frac{1}{2}}_0 = L\frac{dI^{n+\frac{1}{2}}_S}{dt} \tag{3.11}$$

$$I^{n+\frac{1}{2}}_S = I^{n+\frac{1}{2}}_{\frac{1}{2}} + C\frac{dV^{n+\frac{1}{2}}_0}{dt} \tag{3.12}$$

where I_S denotes whole current from source after bias-T, which is relevant to current transmission from both RF and DC source. However, that cannot be directly obtained through iterative process. Substitute Eqn. 3.12 to 3.12, leading to:

$$V^{n+\frac{1}{2}}_S - V^{n+\frac{1}{2}}_0 = L\frac{dI^{n+\frac{1}{2}}_{\frac{1}{2}}}{dt} + LC\frac{d^2V^{n+\frac{1}{2}}_0}{dt^2} \tag{3.13}$$

$$= L\frac{I^{n+1}_{\frac{1}{2}} - I^n_{\frac{1}{2}}}{\Delta t} + LC\frac{V^{n+\frac{3}{2}}_0 - 2V^{n+\frac{1}{2}}_0 + V^{n-\frac{1}{2}}_0}{(\Delta t)^2} \tag{3.14}$$

Then the equation above is rearranged to get an explicit update expression at boundary:

$$V_0^{n+\frac{3}{2}} = (2 - \frac{(\Delta t)^2}{LC})V_0^{n+\frac{1}{2}} - V_0^{n-\frac{1}{2}} + \frac{(\Delta t)^2}{LC}[V_S^{n+\frac{1}{2}} - \frac{L}{\Delta t}(I_{\frac{1}{2}}^{n+1} - I_{\frac{1}{2}}^{n})] \tag{3.15}$$

Initial conditions

Adequate initial conditions play a important role as well to acquire an accurate solution. However, real initial conditions for electrical distribution are not possible to be determined and verified. They can be only analytically set, which means a reasonable station at very beginning. In this case, supposing that QCL was biased by DC source barely at t$\leqslant$ 0, no RF signal has arrived and no lasing yet. The following initial conditions are defined:

$$V_1^0 = V_2^0 = ... = V_j^0 ... = V_N^0 = V_{DC} \tag{3.16}$$

$$I_{j+\frac{1}{2}}^0 = I_S^0 \times \frac{N-j}{N} \quad (j = 0, 1, 2..., N-1) \tag{3.17}$$

where, I_S is the initial current injection, which can be obtained by integrating J(x,0) over x from optical model. N is the amount of nodes while j integer ranging from 0 to N-1. The initial condition for current is under assumption that at very beginning the current was linearly distributed along active region in x direction.

3.2.2 Distributed components

The involvement of transmission line requires distributed component parameters. Except for distributed conductance G', which will be calculated in optical part, distributed resistance R', distributed inductance L' as well as distributed capacitance C' still need to be determined. They can be either calcuted as convertial passive components (plane resistor, parallel plane capacitor and inductor), or extracted from S-Parameter, which can be directly measured with network analyser. The former methode is simple and also don't require any extra test, but could lead to large error due to neglection of fringe effect[26] as well as high frequency influence. The latter is based on experiment, so shows higher accuracy compared with former, but requires extra experiment as well as equipment, which is not always feasible for simulation research.

Distributed resistance

Distributed resistance is frequency dependent and can be obtained by measurement of S-parameter [15], which shows constant value when under certain frequency $R' =$

$4.5 \times 10^{-5}\sqrt{f_{RF}}\,\Omega/mm.$

$$R = \frac{1}{2(w+t)}\sqrt{\frac{\pi\mu f_{RF}}{\sigma}} \tag{3.18}$$

where, t is the thickness of top conductor, μ and σ is the magnetic permeability coefficient and conductivity, respectively. The equation above is obtained by considering the skin effect

–>search corresponding parameters for gold at 77 K.....

Distributed capacitance

The cavity of QC laser is regarded as microstrip line in this case. Quasi-TEM structures, like microstrip, will have frequency dependent impedance and effective dielectric constant. However, if the substrate ($\sim$ 10 um) is thin in terms of wavelength (30 mm $\sim$ 300 mm), and if the strip conductor is very narrow ($\sim$ 50 um) in terms of wavelength, then a static analysis should be perfectly adequate.)

Numerically, one only have to consider a small, bounded 2D region with assumption of uniform cross-section going into the page (See Figure 3.4).

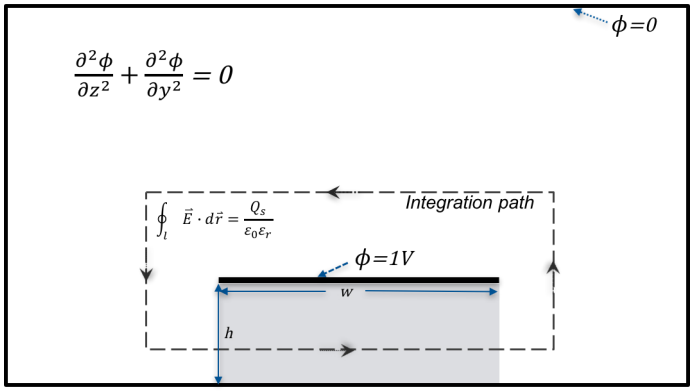

Figure 3.4: *Gauss's 2D equation.*

The electric field can be solved by Gauss's law in 2D. Solving for a strip in a box (Figure 2) the strip potential was set to 1V, the boundary to 0V and solve for the potential at a number of points inside the box. Here an electromagnetic field-solver QuickField was used which is a stand-alone software for solving partial differential equation (PDE).

$$\frac{\partial^2\phi}{\partial y^2} = \frac{\phi_{i-1,j} - 2\phi_{i,j} + \phi_{i+1,j}}{(\Delta y)^2} \tag{3.19}$$

$$\frac{\partial^2\phi}{\partial z^2} = \frac{\phi_{i,j-1} - 2\phi_{i,j} + \phi_{i,j+1}}{(\Delta z)^2} \tag{3.20}$$

Set $\Delta y = \Delta z = \Delta$, then the electrical potential at each grid except top metal layer inside box can be resolved with

$$\phi_{i,j} = \frac{\phi_{i-1,j} + \phi_{i+1,j} + \phi_{i,j-1} + \phi_{i,j+1}}{4\Delta^2}. \tag{3.21}$$

Subsequently, the electrical field can be easily obtained by $E = -\nabla\phi$. With the aid of Matlab electric field on cross-section were calculated as Fig. 3.5 shows. According to

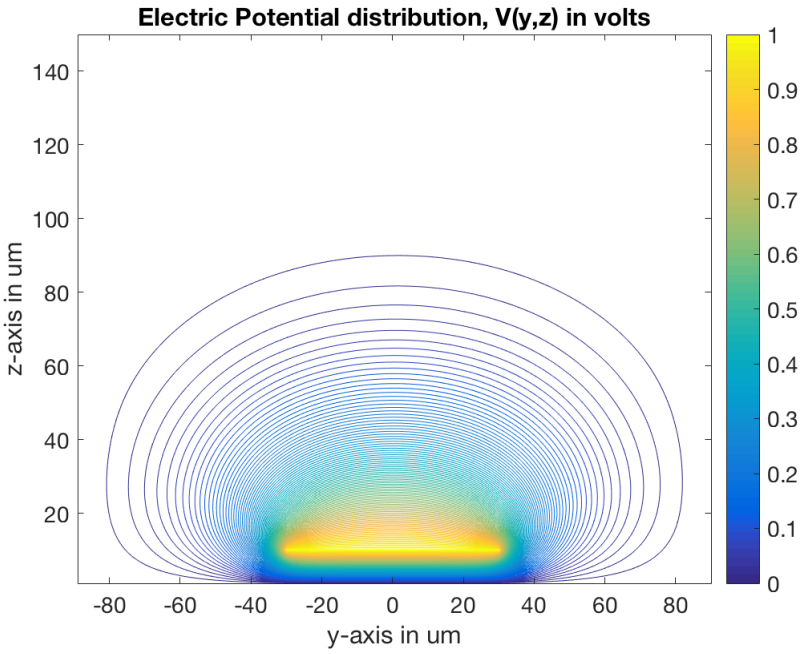

Figure 3.5: *Calculated electrical potential distribution V(y,z) with Matlab.*

Gauss's law in 2D, the surface charge quantity (colon per unit length) can be calculated by integrating the surrounding electric field over arbitrary closed path l with equation

$$Q_S = \oint_l \varepsilon_0 \varepsilon_r \overrightarrow{E} \cdot d\overrightarrow{r} \tag{3.22}$$

where, ε_0 is permittivity in free space and ε_r is relative permittivity of medium, which in this case are air ($\epsilon_r \approx 1$) and semiconductor (active region of QCL, $\epsilon_r \approx 12.96$). Here a rectangular was chosen as integration path for the sake of simplification.

$C = \frac{Q_S}{\phi} = 7.85 \times 10^{-10} F/m$

Distributed inductance

In order to evaluate the self-inductance of surface metal layer in QCLs, Biot–Savart law [27] is used for computing resultant magnetic field **B** (SI unit: Tesla) at surrounding which is generated by a steady current **I**. The distributed inductance L is inhere

characteristic for a certain metal or wire, and is independent of applied current value.

$$\mathbf{B} = \frac{\mu_0}{4\pi}\int_C \frac{Id\mathbf{l}\times\mathbf{r}}{|\mathbf{r}|^3} \tag{3.23}$$

where **l** is the current unit length and **r** is the displacement vector from current unit to the computed point, C is the path that current flows. Boldface denotes that symbols are vector quantities.

In QCLs with metal-metal structure, the thickness of top metal is usually extremely thin which is around 80 nm ($8\times10^{-8}m$). Therefore, it can be regarded as a current sheet with assumption of no thickness (See Fig. 3.6). The magnetic field resulting from a current unit is $d\mathbf{B}_P = \frac{\mu\mathbf{I}\times\mathbf{r}dS}{4\pi wr^3}$ while the magnetic field at a point $\mathbf{B}_P$ results from the magnetic field of each current unit. Hence, it can be evaluated by adding all these together with superposition principle:

$$\mathbf{B}_P = \sum_{i=1}^{n}\sum_{j=1}^{n}\frac{\mu\mathbf{I}\times\mathbf{r}_{i,j}\Delta S}{4\pi w r_{i,j}^3} \tag{3.24}$$

$$= \int_{-\frac{w}{2}}^{\frac{w}{2}}\int_{-\frac{l}{2}}^{\frac{l}{2}}\frac{\mu\mathbf{I}\times\mathbf{r}_{i,j}}{4\pi w r_{i,j}^3}dxdy \tag{3.25}$$

where, w is width of lateral cross section and **r** is vector pointing from the surface element to the observation point P, μ is permeability depending on given medium and frequency.

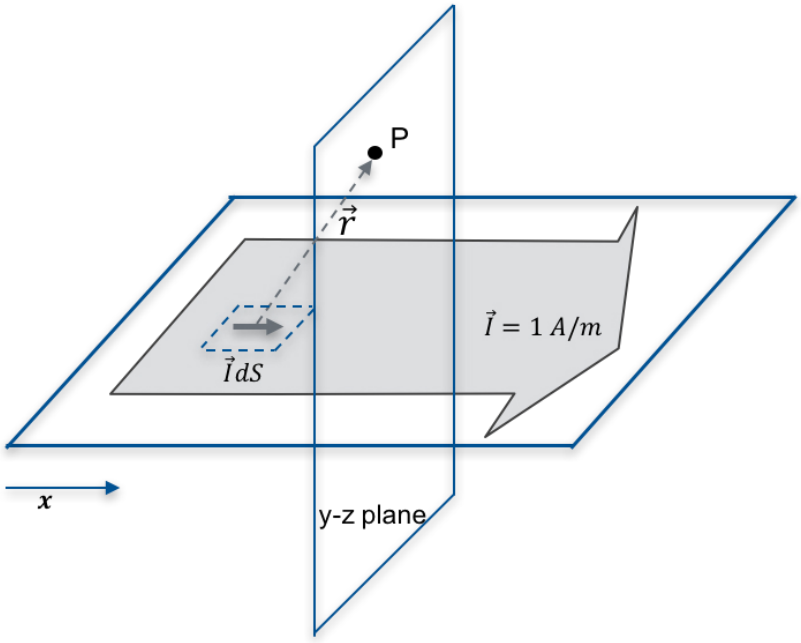

Figure 3.6: *The vector $\vec{r}$ pointing from the surface element to the observation point.*

With formula (3.25) the magnetic field at each point on y-z plane can be solved through either analytical solution or Matlab solution. The energy of inductor can be calculated by following equation:

$$W = \frac{1}{2}LI^2 = \frac{1}{2}\int_{\Omega} BHd\Omega \tag{3.26}$$

where **H** is the auxiliary magnetic field and has a relation $\mathbf{B} = \mu\mathbf{H}$.

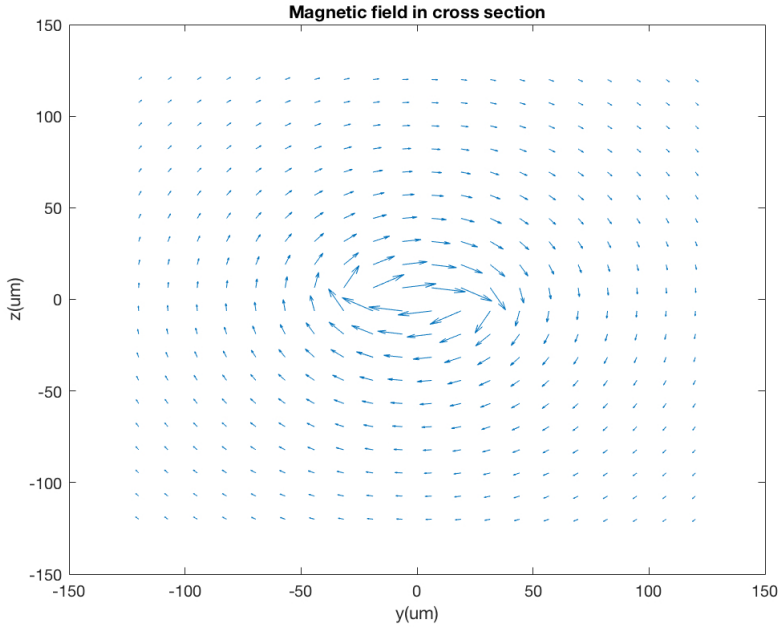

Figure 3.7: *Magnetic feld in cross section y-z plane.*

pictures and calculation.... use the function quiver of Matlab to plot our vector plot. In active region, $\mu \approx \mu_0$, $L' = \frac{\psi}{I} = 3.03 \times 10^{-9} H/m$

$L' = \frac{1}{c^2 C'} = 1.42 \times 10^{-8} H/m$ where c is the speed of light in vacuum.

4 Numerical Treatment

4.1 Discretization

Following Yee's staggered grid approximation[28], voltage and current are discretized with separation of $\Delta x/2$ and $\Delta t/2$ in space and time respectively (See Figure 4.1), which leads to a second-order accurate approximation. Voltage V(x,t) and current I(x,t) samples are then expressed as $V\left(j\Delta x, (n+\frac{1}{2})\Delta t\right)$ and $I\left((j+\frac{1}{2})\Delta x, n\Delta t\right)$, where j and n are integers. For reasons of simplicity, in the following text they will be replaced by $V_j^{n+\frac{1}{2}}$ and $I_{j+\frac{1}{2}}^n$. After discretization, the first-order derivative of voltage $\partial V(x,t)$ as well as current $\partial I(x,t)$ in space and time can be simply calculated with central difference method[29].

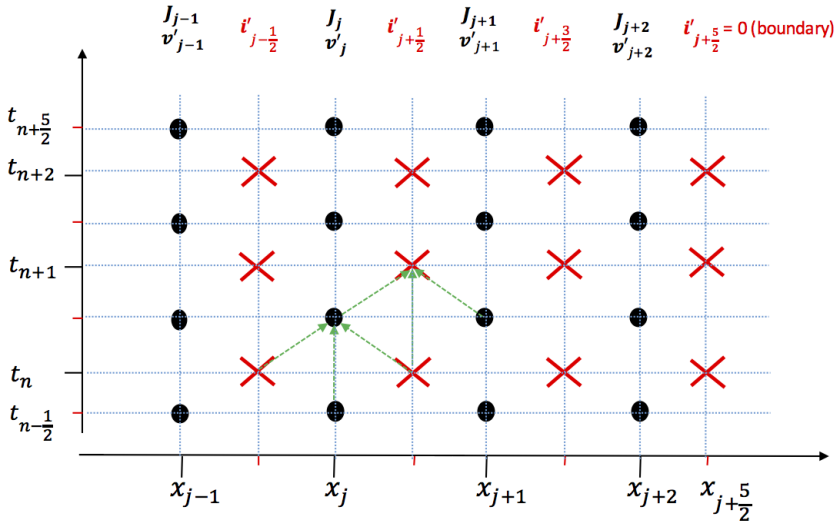

Figure 4.1: *Discretization along a staggered temporal and spatial grid.*

In order to solve these two partial differential equations, finite difference in time domain (FDTD) method is applied which owns second order accuracy.

Subsequently, the original Telegrapher's equations (2.1) and (2.2) are constructed as:

$$\frac{V_{j+1}^{n+\frac{1}{2}} - V_j^{n+\frac{1}{2}}}{\Delta x} \approx -L' \frac{I_{j+\frac{1}{2}}^{n+1} - I_{j+\frac{1}{2}}^{n}}{\Delta t} - R' \widetilde{i}_{j+\frac{1}{2}}^{n+\frac{1}{2}} \tag{4.1}$$

$$\frac{I_{j+\frac{1}{2}}^{n} - I_{j-\frac{1}{2}}^{n}}{\Delta x} \approx -C' \frac{V_j^{n+\frac{1}{2}} - V_j^{n-\frac{1}{2}}}{\Delta t} - w J_j^n \tag{4.2}$$

where, $\widetilde{i}_{j+\frac{1}{2}}^{n+\frac{1}{2}}$ is the ac (alternating current) component flowing between node j and node j+1 due to external RF source. w denotes width of simulated laser cavity. The ac component plays a major role especially in high frequency case, in which metal shows high resistance due to high frequency while in low frequency its resistance can be neglected. In active mode-locking with RF source, the modulation frequency is usually in order of 10^{10} Hz and metal resistance can reach several Ohms at such high frequency. Therefore, the influence of conductor resistance have to be taken into account to realize good agreement with real case. However, it is not suitable for use of traditional methods like Fourier Transformation (FT), which requires lots of samples in time domain. For this reason, it is not possible in this case to directly separate ac component of high frequency from the whole current during simulation.

Now that pure ac component cannot be simply obtained while resistance of transmission line at high frequency muss be taken into consideration, the problem was solved in another way by compromise. Instead of directly separating ac and dc component, temporal difference of ac component between adjacent time steps is considered to be feasible solution, which can be simply obtained by subtracting of Eqn. (4.1) at time $(n + \frac{1}{2})$ with that equation at previous time step $(n + \frac{1}{2})$, leading to:

$$\frac{V_{j+1}^{n+\frac{3}{2}} - V_j^{n+\frac{3}{2}} - (V_{j+1}^{n+\frac{1}{2}} - V_j^{n+\frac{1}{2}})}{\Delta x} \approx -L' \frac{I_{j+\frac{1}{2}}^{n+2} - 2I_{j+\frac{1}{2}}^{n+1} + I_{j+\frac{1}{2}}^{n}}{\Delta t} - R'(\widetilde{i}_{j+\frac{1}{2}}^{n+\frac{3}{2}} - \widetilde{i}_{j+\frac{1}{2}}^{n+\frac{1}{2}}) \tag{4.3}$$

The idea is, dc component as well as ac component with low frequency remains nearly unchanged after extremly short time step Δt which is shorter than picosecond (10^{-12} second) in the modeling. The variation of whole current at node $j + \frac{1}{2}$ is mainly due to variation of ac component with high frequency, which plays a key roll for increase of metal resistance. Hence, the variation of ac component can be approximately replaced with its corresponding variation of whole current. Besides, the current components have to be averaged in time for sake of consistence, the same with J_j^n, leading to:

$$\widetilde{i}_{j+\frac{1}{2}}^{n+\frac{3}{2}} - \widetilde{i}_{j+\frac{1}{2}}^{n+\frac{1}{2}} \approx I_{j+\frac{1}{2}}^{n+\frac{3}{2}} - I_{j+\frac{1}{2}}^{n+\frac{1}{2}} \approx \frac{I_{j+\frac{1}{2}}^{n+2} + I_{j+\frac{1}{2}}^{n+1} - (I_{j+\frac{1}{2}}^{n+1} + I_{j+\frac{1}{2}}^{n})}{2} \tag{4.4}$$

Then substituting the approximate treatment above to Eqn. (4.3), a equation with only voltage and whole current can be obtained:

$$\frac{V_{j+1}^{n+\frac{3}{2}} - V_j^{n+\frac{3}{2}} - (V_{j+1}^{n+\frac{1}{2}} - V_j^{n+\frac{1}{2}})}{\Delta x} \approx -L' \frac{I_{j+\frac{1}{2}}^{n+2} - 2I_{j+\frac{1}{2}}^{n+1} + I_{j+\frac{1}{2}}^{n}}{\Delta t} - R' \frac{I_{j+\frac{1}{2}}^{n+2} - I_{j+\frac{1}{2}}^{n}}{2} \quad (4.5)$$

Finally, after rearrangement a recursive solution for Transmission line updating are explicitly expressed as:

$$I_{j+\frac{1}{2}}^{n+2} = \frac{4L'}{2L' + R'\Delta t} I_{j+\frac{1}{2}}^{n+1} - \frac{2L' - R'\Delta t}{2L' + R'\Delta t} I_{j+\frac{1}{2}}^{n} + \frac{V_{j+1}^{n+\frac{3}{2}} - V_j^{n+\frac{3}{2}} - V_{j+1}^{n+\frac{1}{2}} + V_j^{n+\frac{1}{2}}}{(\frac{L'}{\Delta t} + \frac{R'}{2})\Delta x} \quad (4.6)$$

$$V_j^{n+\frac{1}{2}} = V_j^{n-\frac{1}{2}} + \frac{\Delta t}{C'\Delta x}(I_{j-\frac{1}{2}}^{n} - I_{j+\frac{1}{2}}^{n} - w\Delta x \frac{J_j^{n+\frac{1}{2}} + J_j^{n-\frac{1}{2}}}{2}) \quad (4.7)$$

In the recursive equations above, except for the distributed parameters (R', L', C') time step Δt and space step Δx are still needed to be determined. Theoretically the smaller these step values were set, the more accurate their solution will be. But in real computation it wouldn't be chosen unlimited small, therefore, "magic time step" [30] is taken with regarding to stability, which is expressed as

$$\Delta t = n\Delta x/c = n\sqrt{\epsilon\mu}\Delta x, \quad (4.8)$$

where n is the refractive index of active region.

4.2 Modulation power

Not only modulation frequency but also modulation power plays a key role in mode-locking. Even if QCL was modulated at near roundtrip frequency f_{rt} , it can't be mode locked without enough modulation power. So it is essential to evaluate RF power for each simulation in order to analyze the modulation process. The RF source power can be easily calculated as modulation amplitude, signal function (since wave) as well as frequency are all known. But this power is total power and is larger than the power that was injected into QCL. Only the injected RF power will have influence on modulation.

The reflection coefficient Γ is defined as:

$$\Gamma = \frac{Z_{QCL} - Z_S}{Z_{QCL} + Z_S} \quad (4.9)$$

Two methods could be used to estimate modulation power:

1. Through Fourier Transformation ac component can be easily separated at modulation frequency f_{RF} from recorded whole current data over time. In the way, average RF voltage signal can also be obtained. Therefore, the injected RF-power to QCL is approximately:

$$P_{RF} = \delta I * \delta V. \tag{4.10}$$

Where δI and δV are current and voltage components with frequency of f_{RF}, respectively. They can be obtained by Fourier Transform of recorded data after simulation. The calculated value in this way should larger than real injected RF power, because even without RF source the laser itself has also current and voltage components with the same frequency f_{RF} due to microstrip line.

2. The impedance of transmission line (in this case QCL) at certain frequency is

$$Z_{QCL} = \sqrt{\frac{R' + j2\pi f_{RF} L'}{G' + j2\pi f_{RF} C'}}. \tag{4.11}$$

For calculation of small signal current modulation, there is a formula [31] can be used

$$P_{diss} = \frac{\delta I_{QCL}^2 * Re[Z_{QCL}]}{2}. \tag{4.12}$$

Where δI_{QCL} is induced current variation due to RF source. The distributed conductance G′ can be obtained through I-V characteristic curve of QCL.

5 Simulation Results

The laser simulated in this work is based on doped $GaAs/Al_xGa_{1-x}As$, which is 3 mm-long, 60 μm wide, with height of 10 μm metal-metal QCL. It is driven at 77 K and has an emission frequency of 3.8 THz. The average doping level of the active region is $5 \times 10^{16} cm^3$. Its well and barrier widths are 4.6/9.8/2.6/9.0/4.4/17.6 nm.

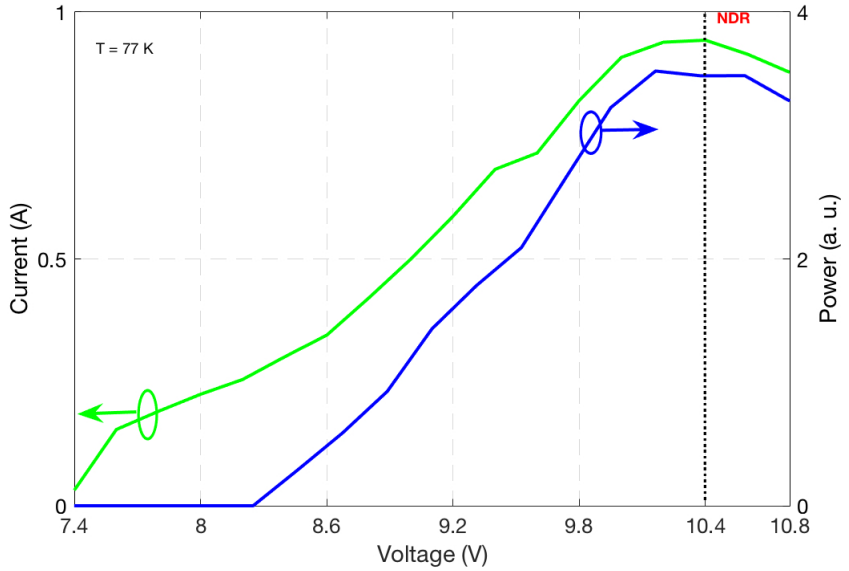

Figure 5.1: *voltage-current–power characteristics of simulated QCL.*

Fig. 5.1 shows the voltage-current–power characteristics of the QCL, which was obtained by simulating the QCL under a series of bias from 7.4 V to 10.8 V. The QCL has a threshold voltage V_{th} of 8.4 V, which means, under that there will be no lasing. Starting from V_{th}, the output power will increase exponentially with higher voltage until tunneling phenomena occurs. At this area, QCL owns negative differential resistance (NDR) which is similar as tunneling diode. A large amount of injected electrons due to increased input voltage will directly pass active region through tunneling rather than transition from upper and lower laser levels accompanied with emission of phonons. Therefore, they will not contribute to laser output power. –> kink?

In order to obtain a accuracy roundtrip frequency of this QCL, beatnote was used by Fourier transform of its output power. As Fig. 5.2 shows the beatnote of simulated QCL without modulation, its roundtrip frequency f_{rt} is about 13.34 GHz.

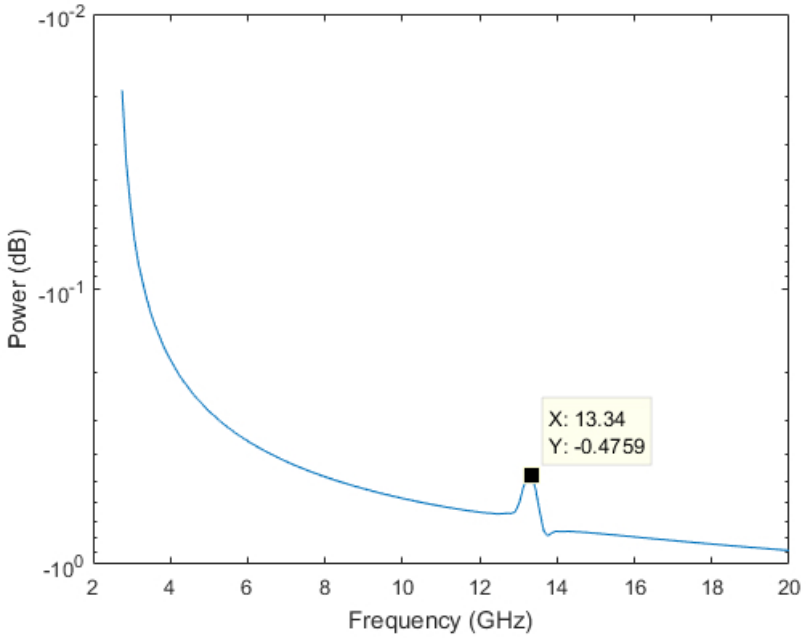

Figure 5.2: *Beatnote of the QCL without modulation.*

Table 5.1: *Simulation parameters*

Name	Symbol	Value	Unit
Cavity length	L_{tot}	3	mm
Cavity width	w	60	um
Doping density	D_p	1.5E16	cm^{-3}
Period length	L_p	54.8	nm
Overlap factor	Γ	0.8	
Cavity loss	L_α	13	$1/cm$

5.1 Simulation setup

The source of simulated QCL consists of a DC voltage source and a RF source, which are combined through bias-T. The QCL is biased by DC source and modulated by RF source. Both source are chose as voltage source for continence. The modulation signal of RF source has a function

$$V_{RF} = modA \sin(2\pi f_{RF} t), \tag{5.1}$$

where modA is voltage amplitude of RF source.

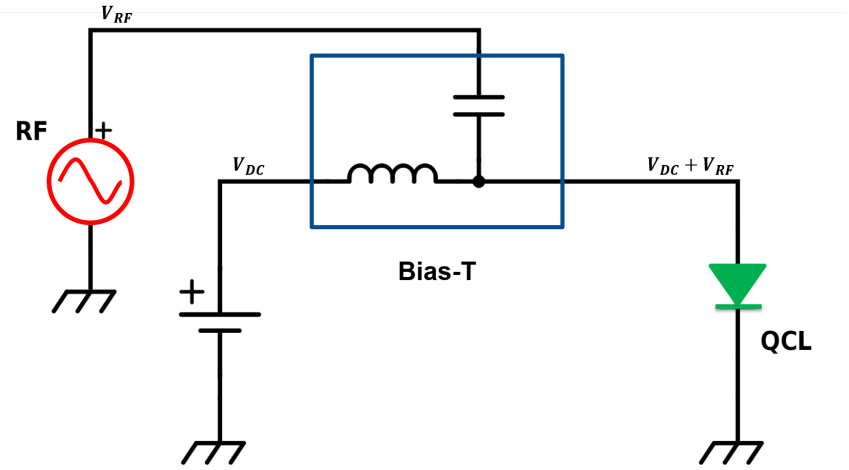

Figure 5.3: *Schematic scheme of simulation setup.*

5.2 Results

A series of simulations were carried out for investigating the influence of modulation power as well frequency on mode-locking of QCLs. After 200 roundtrips simulation, a clear short pulse was observed, as Figure 5.4 shows, from 4610 to 4690 ps in corresponding to 164 roundtrip time T_{rt}. Its Full Width at Half Maximum (FWHM) in this modeling is around 11.6 ps, which shows quite good agreement with experiment result 11 ps [11].

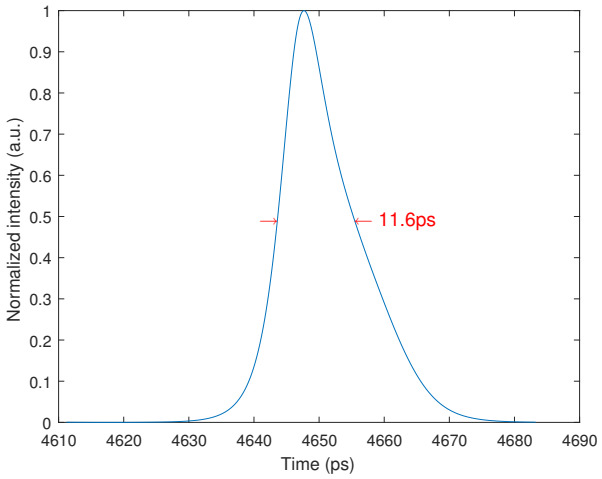

Figure 5.4: *Singel pulse from simulation.*

5.2.1 Modulation with different power

Before simulation was carried out, their rough values (modA and f_{RF}) have to be firstly determined. Although the RF source function is known (Eq. (5.1)) and its power is proportional to square of modA, the injected power to QCL can still not be determined before simulation. Due to reflection as well as attenuation on wire between RF source and QCL, the injected power should be smaller than the power coming from RF source. But it is well known that theoretically optimal modulation frequency should exactly at roundtrip frequency. Therefore, simulations with different power and certain f_{RF} were firstly carried out.

Lack of sufficient modulation power, QCLs can still not be mode-locked even if modulation frequency is equal to f_{rt}. Therefore, modulations with different RF amplitude (modA) was investigated, which haven the same modulation frequency and all other parameters are the same as well. When without RF source, QCL emits continuous light and will show a clear single peak in frequency domain, which is its emission frequency. The left graph of Fig. 5.5 is pulse trains with five roundtrips and right graph shows their corresponding frequency spectra. With increasing modulation power the side modes near main mode were strengthened and contributed to form short pulses. At modA which equals to 4 V, clear short pulse train was observed. This valued would be further used for investigating locking range of the QCL.

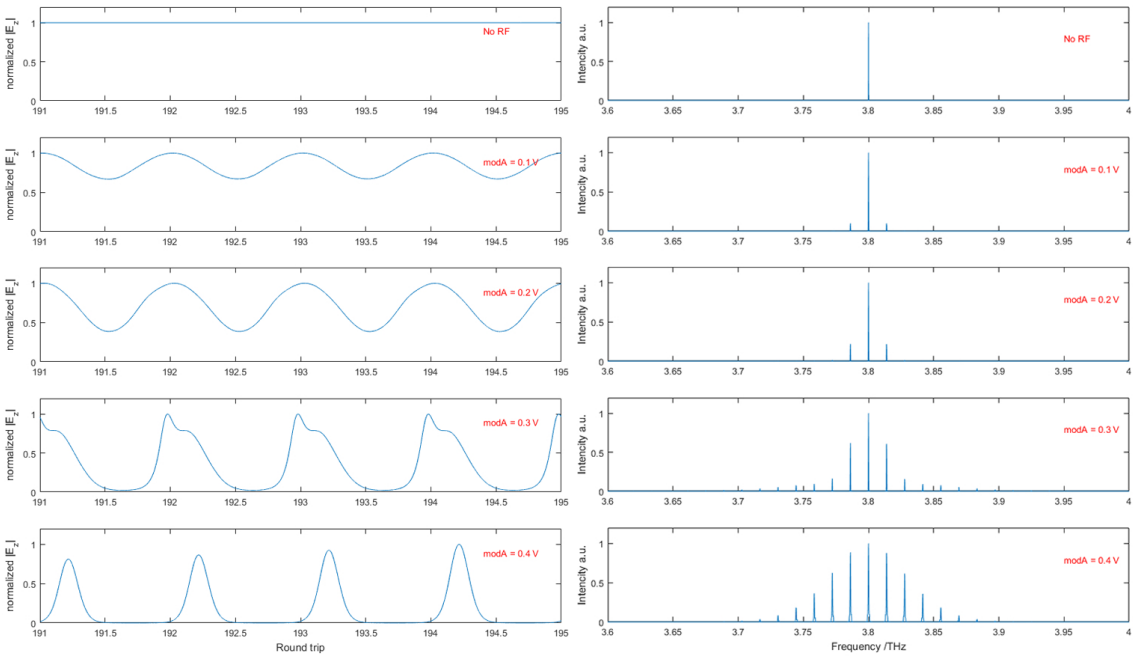

Figure 5.5: *Normalized spectra in time as well as frequency domain with different modulation powers. modA denotes RF amplitude. f_{RF} of RF source is at roundtrip frequency and QCL is bias by 8.6 kV/cm*

5.2.2 Modulation with different frequency

Modulation frequency is a key factor for mode-locking. As already discussed at chapter 2.3 Mode-locking, the modulation frequency has to be close to roundtrip frequency. To investigate its maximal possible locking range, the laser was modulated with a large frequency interval nearby f_{rt}.

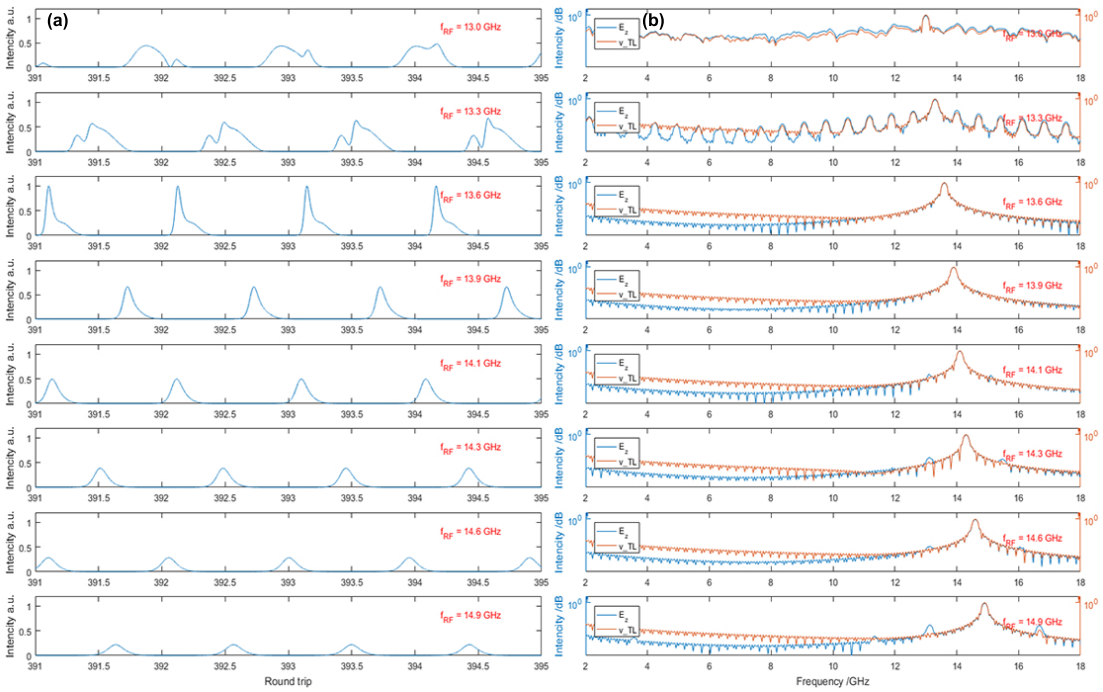

Figure 5.6: *Frequency spectra with different modulation powers.*

Fig. 5.6(a) shows pulse trains at time domain at a series of modulation frequencis from 13 GHz to 14.9 GHz, its time axis was normalized in roundtrips. This was obtained by recording the optical field E_z in the middle point (x=L/2) of QCL at each time step and the last 5 roundtrips were chose to check their pulse shapes. Besides, their power intensity (proportional to $|E_z^2|$) were then normalized to the one which has highest intensity in order to compare their relative emission power. The shortest pulses were found at modulation frequency 13.6 GHz and 13.9 GHz, which have FWHM of 10.7 ps and 11.2 ps, respectively. This can also be verified by the right graph beatnote (Fig. 5.6(b)), which contains not only optical power but also voltage signal of QCL in frequency domain. From 13.6 GHz to 13.9 GHz their frequency spectra of optical power and electrical voltage matched completely. Over this range some modes appeared which are not coherent with the other modes and disturbed mode-locking.

5.3 Comparison with experiment

Compared with experiment results from Ref. [32], which used the same QCL as in this work, the obtained pulse width (FWHM) 11.6 ps is almost the same as from experiment, which shows good agreement.

Locking range:

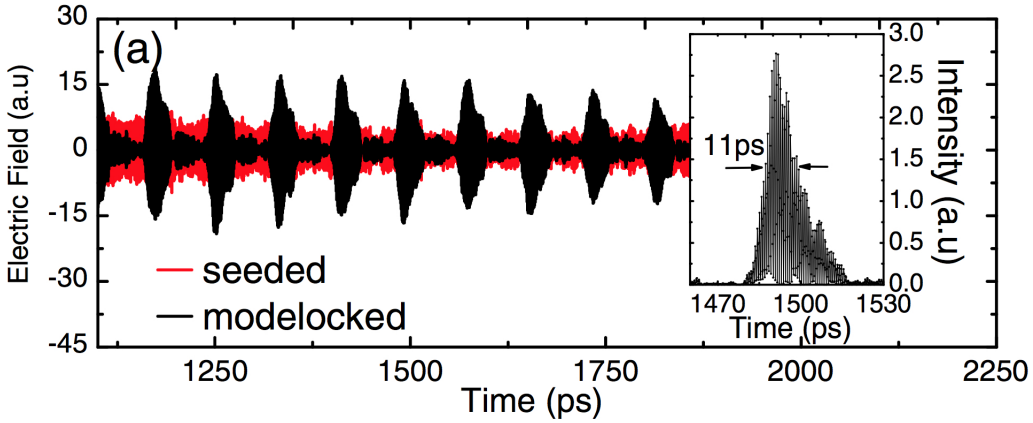

Figure 5.7: *Experiment data from Ref. [32]: output electric field for the seeded (red) and mode-locked (black) QCLs with an applied microwave modulation of 12.46 GHz for the latter. Inset: expanded view of the THz pulse intensity between 1470 and 1530 ps.*

6 Conclusion

Bibliography

[1] R. Kazarinov, "Possibility of amplification of electromagnetic waves in a semiconductor with superlattice," *Sov. Phys.-Semicond.*, vol. 5, no. 4, pp. 707–709, 1971. *Cited on page 1.*

[2] J. Faist, F. Capasso, D. L. Sivco, C. Sirtori, A. L. Hutchinson, and A. Y. Cho, "Quantum cascade laser," *Science*, vol. 264, no. 5158, pp. 553–556, 1994. *Cited on page 1.*

[3] B. S. Williams, "Terahertz quantum-cascade lasers," *Nature photonics*, vol. 1, no. 9, pp. 517–525, 2007. *Cited on page 1.*

[4] C. Gmachl, D. L. Sivco, R. Colombelli, F. Capasso, and A. Y. Cho, "Ultra-broadband semiconductor laser," *Nature*, vol. 415, no. 6874, pp. 883–887, 2002. *Cited on page 1.*

[5] J. F. Federici, B. Schulkin, F. Huang, D. Gary, R. Barat, F. Oliveira, and D. Zimdars, "Thz imaging and sensing for security applications—explosives, weapons and drugs," *Semiconductor Science and Technology*, vol. 20, no. 7, p. S266, 2005. *Cited on page 1.*

[6] Y. Bai, N. Bandyopadhyay, S. Tsao, S. Slivken, and M. Razeghi, "Room temperature quantum cascade lasers with 27% wall plug efficiency," *Applied Physics Letters*, vol. 98, no. 18, p. 181102, 2011. *Cited on page 1.*

[7] C. Y. Wang, L. Kuznetsova, V. Gkortsas, L. Diehl, F. X. Kaertner, M. A. Belkin, A. Belyanin, X. Li, D. Ham, H. Schneider, *et al.*, "Mode-locked pulses from mid-infrared quantum cascade lasers," *Optics express*, vol. 17, no. 15, pp. 12929–12943, 2009. *Cited on pages 1 and 2.*

[8] D. Revin, M. Hemingway, Y. Wang, J. Cockburn, and A. Belyanin, "Active mode locking of quantum cascade lasers in an external ring cavity," *Nature communications*, vol. 7, 2016. *Cited on page 2.*

[9] N. Vukovic, J. Radovanovic, V. Milanovic, and D. L. Boiko, "Low-threshold rngh instabilities in quantum cascade lasers," *arXiv preprint arXiv:1601.03212*, 2016. *Cited on page 2.*

[10] S. Barbieri, M. Ravaro, P. Gellie, G. Santarelli, C. Manquest, C. Sirtori, S. P. Khanna, E. H. Linfield, and A. G. Davies, "Coherent sampling of active mode-locked terahertz quantum cascade lasers and frequency synthesis," *Nature Photonics*, vol. 5, no. 5, pp. 306–313, 2011. *Cited on page 2.*

[11] P. Gellie, S. Barbieri, J.-F. Lampin, P. Filloux, C. Manquest, C. Sirtori, I. Sagnes, S. P. Khanna, E. H. Linfield, A. G. Davies, *et al.*, "Injection-locking of terahertz quantum cascade lasers up to 35ghz using rf amplitude modulation," *Optics express*, vol. 18, no. 20, pp. 20799–20816, 2010. *Cited on pages 2 and 27.*

[12] C. Wang, F. Grillot, V. Kovanis, and J. Even, "Rate equation analysis of injection-locked quantum cascade lasers," *Journal of Applied Physics*, vol. 113, no. 6, p. 063104, 2013. *Cited on page 2.*

[13] H. Yasuda, T. Kubis, P. Vogl, N. Sekine, I. Hosako, and K. Hirakawa, "Nonequilibrium green's function calculation for four-level scheme terahertz quantum cascade lasers," *Applied Physics Letters*, vol. 94, no. 15, p. 151109, 2009. *Cited on page 2.*

[14] S. Barbieri, W. Maineult, S. S. Dhillon, C. Sirtori, J. Alton, N. Breuil, H. E. Beere, and D. A. Ritchie, "13 ghz direct modulation of terahertz quantum cascade lasers," *Applied Physics Letters*, vol. 91, no. 14, p. 143510, 2007. *Cited on page 2.*

[15] W. Maineult, L. Ding, P. Gellie, P. Filloux, C. Sirtori, S. Barbieri, T. Akalin, J.-F. Lampin, I. Sagnes, H. Beere, *et al.*, "Microwave modulation of terahertz quantum cascade lasers: a transmission-line approach," *Applied Physics Letters*, vol. 96, no. 2, p. 021108, 2010. *Cited on pages 2 and 15.*

[16] B. Jonsson and S. T. Eng, "Solving the schrodinger equation in arbitrary quantum-well potential profiles using the transfer matrix method," *IEEE journal of quantum electronics*, vol. 26, no. 11, pp. 2025–2035, 1990. *Cited on page 5.*

[17] I.-H. Tan, G. Snider, L. Chang, and E. Hu, "A self-consistent solution of schrödinger–poisson equations using a nonuniform mesh," *Journal of applied physics*, vol. 68, no. 8, pp. 4071–4076, 1990. *Cited on page 5.*

[18] O. Heaviside, *Electromagnetic theory*, vol. 3. Cosimo, Inc., 2008. *Cited on page 5.*

[19] H. A. Haus, "Mode-locking of lasers," *IEEE Journal of Selected Topics in Quantum Electronics*, vol. 6, no. 6, pp. 1173–1185, 2000. *Cited on page 7.*

[20] X. Huang, Y. Dikmelik, and C. Gmachl, "Non-uniform lateral current distribution in quantum cascade lasers," *Optics express*, vol. 22, no. 5, pp. 6154–6164, 2014. *Cited on page 9.*

[21] R. Dhar and D. Ban, "Nanoscopic voltage distribution of operating cascade laser devices in cryogenic temperature," *Journal of microscopy*, 2015. *Cited on page 9.*

[22] Y. Xu, R. Gwoziecki, I. Chartier, R. Coppard, F. Balestra, and G. Ghibaudo, "Modified transmission-line method for contact resistance extraction in organic field-effect transistors," *Applied Physics Letters*, vol. 97, no. 6, p. 171, 2010. *Cited on page 12.*

[23] N. Johnston, M. Pan, and S. Kudzma, "An enhanced transmission line method for modelling laminar flow of liquid in pipelines," *Proceedings of the Institution of Mechanical Engineers, Part I: Journal of Systems and Control Engineering*, vol. 228, no. 4, pp. 193–206, 2014. *Cited on page 12.*

[24] C. Yan, Q. J. Wang, L. Diehl, M. Hentschel, J. Wiersig, N. Yu, C. Pflügl, F. Capasso, M. A. Belkin, T. Edamura, *et al.*, "Directional emission and universal far-field behavior from semiconductor lasers with limaçon-shaped microcavity," *Applied Physics Letters*, vol. 94, no. 25, p. 251101, 2009. *Cited on page 12.*

[25] A. Orlandi and C. R. Paul, "Fdtd analysis of lossy, multiconductor transmission lines terminated in arbitrary loads," *IEEE Transactions on Electromagnetic Compatibility*, vol. 38, no. 3, pp. 388–399, 1996. *Cited on page 13.*

[26] K. Pillai, "Fringing field of finite parallel-plate capacitors," in *Proceedings of the Institution of Electrical Engineers*, vol. 117, pp. 1201–1204, IET, 1970. *Cited on page 15.*

[27] I. S. Grant and W. R. Phillips, *Electromagnetism*. John Wiley & Sons, 2013. *Cited on page 17.*

[28] K. Yee, "Numerical solution of initial boundary value problems involving maxwell's equations in isotropic media," *IEEE Transactions on antennas and propagation*, vol. 14, no. 3, pp. 302–307, 1966. *Cited on page 21.*

[29] D. Yang, P. Tong, and X. Deng, "A central difference method with low numerical dispersion for solving the scalar wave equation," *Geophysical Prospecting*, vol. 60, no. 5, pp. 885–905, 2012. *Cited on page 21.*

[30] K. Li, M. Tassoudji, R. Shin, and J. Kong, "Simulation of electromagnetic radiation and scattering using a finite difference-time domain technique," *Computer Applications in Engineering Education*, vol. 1, no. 1, pp. 45–63, 1992. *Cited on page 23.*

[31] S. Ramo, J. R. Whinnery, and T. Van Duzer, *Fields and waves in communication electronics*. John Wiley & Sons, 2008. *Cited on page 24.*

[32] F. Wang, K. Maussang, S. Moumdji, R. Colombelli, J. R. Freeman, I. Kundu, L. Li, E. H. Linfield, A. G. Davies, J. Mangeney, *et al.*, "Generating ultrafast pulses of light from quantum cascade lasers," *Optica*, vol. 2, no. 11, pp. 944–949, 2015. *Cited on page 30.*